

EFFICIENT GABOR FILTER DESIGN FOR TEXTURE SEGMENTATION

Thomas P. Weldon, William E. Higgins*, and Dennis F. Dunn†

Department of Electrical Engineering, University of North Carolina, Charlotte, NC 28262

*Department of Electrical Engineering, Penn State University, University Park, Pennsylvania 16802

†Department of Computer Science and Engineering, Penn State University, University Park, Pennsylvania 16802

Abstract

Gabor filters have been successfully applied to a broad range of image processing tasks. The present paper considers the design of a single filter to segment a two-texture image. A new efficient algorithm for Gabor-filter design is presented, along with methods for estimating filter output statistics. The algorithm draws upon previous results that showed that the output of a Gabor-filtered texture is modeled well by a Rician distribution. A measure of the total output power is used to select the center frequency of the filter and is used to estimate the Rician statistics of the Gabor-filtered image. The method is further generalized to include the statistics of postfiltered outputs that are generated by a Gaussian filtering operation following the Gabor filter. The new method typically requires an order of magnitude less computation to design a filter than a previously proposed method. Experimental results demonstrate the efficacy of the method.

Image segmentation Texture Gabor filters Rician statistics Texture segmentation Image statistics
Texture analysis

1. INTRODUCTION

¹Gabor filters have been successfully applied to many image-processing applications, such as texture segmentation,⁽¹⁻⁸⁾ document analysis,⁽⁹⁾ edge detection,⁽¹⁰⁾ retina identification,⁽¹¹⁾ fingerprint processing,⁽¹²⁾ image coding,^(13,14) and image representation.⁽¹⁵⁾ An advantage of these filters is that they satisfy the minimum space-bandwidth product per the uncertainty principle. Hence, they provide simultaneous optimal resolution in both the space and spatial-frequency domains.⁽¹⁶⁾ Further, they are bandpass filters, conforming well to mammalian visual receptive field profiles.^(1,2,16) Generally speaking, people use Gabor filters when trying to solve problems involving complicated images comprised of textured regions. We consider the problem of segmenting textured images in this paper. (For a more complete review on the research issues in Gabor filter design for texture segmentation, consult Dunn *et al.*^(6,7))

A central issue in applying these filters to texture segmentation is the determination of the filter parameters. Daugman considered a filter-bank wavelet decomposition based on biological vision.⁽¹³⁾ A subset of a similar filter-bank was proposed by Jain and Farrokhnia.⁽³⁾ One difficulty with this approach is that the filter parameters are preset and are not necessarily optimal for a particular processing task. Also, some segmentation tasks may not require a bank of filters or may not tolerate the additional computational burden. Recent work presented an approach that uses one Gabor filter per texture.^(1,2) The center frequency of each filter was selected to correspond to a peak in the texture power spectrum, and filter bandwidths were determined by the center frequency. Another effort provided a detailed treatment of the optimal design of a single Gabor filter to segment two textures.^(5,7) The method involved an exhaustive search to find the center frequency, and the image-segmentation error was minimized using measured output statistics and a Rician statistical model.

This paper further considers the issue of designing a single Gabor filter for discriminating between two textures (the texture segmentation problem). Although the method we propose is limited to the design of a

¹Elsevier is liberal with respect to authors and electronic preprints. Unlike some publishers, we do not consider that a preprint of an article (including a prior version as a thesis) prior to its submission to Elsevier for consideration amounts to prior publication, which would disqualify the work from consideration for re-publication in a journal. We also do not require authors to remove electronic preprints from publicly accessible servers (including the author's own home page) once an article has been accepted for publication. (www.elsevier.com)

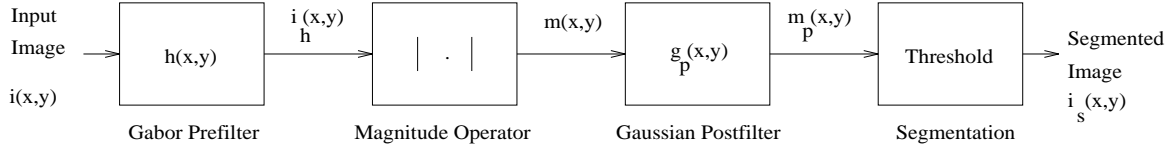


Figure 1: Image processing block diagram.

single Gabor filter to segment two textures, the underlying principles provide an important foundation for ongoing research to develop more general methods for designing multiple Gabor filters to segment multiple textures.^(17,18) Further, the limitation of the proposed method to two textures does not necessarily rule out useful applications, since the segmentation of text from pictures in documents has been successfully approached using texture-segmentation methods.^(9,19)

Key features of the new method include a reduction in computational complexity by an order of magnitude over the previously proposed approach and a method for estimating the output statistics of the filtered textures.^(5,7) Although computational complexity of the filter design method does not affect all applications, it does become important when operator-interaction is desired in the design process. The computational complexity of a single-filter design procedure may become critical when addressing the multi-filter design problem with the accompanying combinatorial expansion in *filter combinations*. The new method also places no restrictions on the textures. Finally, the designed filter is optimal in the sense that it maximizes the expected ratio of average output energy for the two prefiltered textures.

Part 2 first reviews the assumed image-processing framework. In Part 3, we propose a Gabor-filter design technique, based on autocorrelation measurements, that is computationally more efficient than previous methods.^(5,7) Then, in Part 4, we provide a method for estimating the pdf of the Gabor filter output using a Rician model. The estimated pdf's are used to establish a threshold that minimizes the image-segmentation error. Further, we consider the use of a Gaussian postfilter in the analysis. The Gaussian postfilter, which reduces the variance of the Rician-distributed Gabor-filter output, results in reduced image-segmentation error at the expense of some loss in spatial resolution. To avoid confusion, we will refer to the Gabor filter as the *Gabor prefilter* and the subsequent Gaussian filter as the *Gaussian postfilter*. The results of Part 5 demonstrate that the filter-design algorithm generates effective filters for image segmentation. Moreover, the results show that our methods accurately predict filter-output statistics. We also discuss the computational complexity and performance of the method relative to the previous approach.

2. IMAGE PROCESSING OVERVIEW AND PROBLEM STATEMENT

A block diagram of the fundamental image processing under consideration is shown in Fig. 1. The technique outlined in the figure has been justified for texture segmentation by previous investigators.^(1,2,6) Below, we provide an overview of the image processing in Fig. 1 and define the filter-design problem.

The input image $i(x, y)$ is assumed to be composed of two textures, as will be discussed in Part 3. The image is first passed through a Gabor prefilter with impulse response $h(x, y)$, where

$$h(x, y) = g(x, y) e^{-j2\pi(Ux+Vy)}$$

and

$$g(x, y) = \frac{1}{2\pi\sigma_g^2} e^{-\frac{(x^2+y^2)}{2\sigma_g^2}}. \quad (1)$$

The *Gabor function* $h(x, y)$ is a complex sinusoid centered at frequency (U, V) and modulated by a Gaussian envelope $g(x, y)$. The spatial extent of the Gaussian envelope is determined by parameter σ_g . Further, the 2-D Fourier transform of $h(x, y)$ is

$$H(u, v) = G(u - U, v - V) \quad (2)$$

where

$$G(u, v) = e^{-2\pi^2\sigma_g^2(u^2+v^2)} \quad (3)$$

is the Fourier transform of $g(x, y)$. The parameters (U, V, σ_g) determine $h(x, y)$. From (2-3), we see that the Gabor function is essentially a bandpass filter centered about frequency (U, V) , with bandwidth determined by σ_g . We assume for simplicity that the Gaussian envelope $g(x, y)$ is a symmetrical function. Other treatments have considered the impact of an asymmetrical Gaussian envelope.⁽⁶⁾

The output of the prefilter stage $i_h(x, y)$ is the convolution of the input image with the filter response

$$i_h(x, y) = h(x, y) * i(x, y) .$$

where $*$ denotes convolution in two dimensions. The magnitude of the first-stage output is computed in the second stage as

$$m(x, y) = |i_h(x, y)| = |h(x, y) * i(x, y)| . \quad (4)$$

A low-pass Gaussian postfilter $g_p(x, y)$ is applied to prefilter output $m(x, y)$ yielding the postfiltered image

$$m_p(x, y) = m(x, y) * g_p(x, y) , \quad (5)$$

where

$$g_p(x, y) = \frac{1}{2\pi\sigma_p^2} e^{-\frac{(x^2+y^2)}{2\sigma_p^2}} . \quad (6)$$

Generally, we will refer to $i_h(x, y)$ as the prefiltered image, $m(x, y)$ as the prefilter output, and $m_p(x, y)$ as the postfilter output.

Post-filtering (5) was used by previous investigators to smooth out variations in $m(x, y)$.^(1,5,7) Further discussion on this will be given in Part 4. The final step in Fig. 1 is to generate the segmented image $i_s(x, y)$ from the Gaussian-postfilter output $m_p(x, y)$. To do this, we apply a threshold τ to $m_p(x, y)$; points above the threshold are assigned to one texture, and points below to the other. More elaborate segmentation techniques can be employed, but a simple threshold directly demonstrates the effectiveness of the new methods.

Given the system of Fig. 1, we now state the Gabor prefilter design problem. Consider the input image $i(x, y)$ to be composed of disjoint regions of two dissimilar textures, $t_1(x, y)$ and $t_2(x, y)$. Then the problem is to find the Gabor function $h(x, y)$ that provides the greatest discrimination between the two textures in the filtered image $m_p(x, y)$.

Our approach to the problem is as follows. Using a statistical model for $i(x, y)$, find the Gabor function $h(x, y)$ that maximizes the ratio of Gabor-prefilter output power for the two textures. Then, upon applying a Gaussian postfilter, use the predicted statistics of the postfilter output $m_p(x, y)$ to determine a threshold that minimizes the image-segmentation error in the final segmented image $i_s(x, y)$. Parts 3 and 4 outline the analytical arguments and design procedures for our approach.

3. FILTER DESIGN ALGORITHM

In this section we propose an algorithm for designing the Gabor prefilter $h(x, y)$ that is more efficient than the previous approach.^(5,7) The proposed method assumes that representative realizations of the two textures are available and draws upon the autocorrelations for each of the two sample textures. The statistics of $m(x, y)$ and $m_p(x, y)$ are discussed in Part 4, along with the effects of Gaussian postfiltering.

We proceed with the development of the filter design algorithm by first establishing a method for simultaneously computing the output power of a large number of candidate Gabor prefilters for a particular texture. This measure of output power is then used to select the best Gabor prefilter, thus establishing the

prefilter parameters. The development proceeds for one texture, and the results are later generalized to both textures.

Recall that the input image $i(x, y)$ is composed of two textures, $t_1(x, y)$ and $t_2(x, y)$. We assume that the given realizations of these two textures are samples from ergodic 2-D random processes. Denote the power spectral densities of $t_1(x, y)$ and $t_2(x, y)$ by $S_1(u, v)$ and $S_2(u, v)$.

When $t_1(x, y)$ is filtered by a Gabor prefilter $h(x, y)$ with fixed parameters (U, V, σ_g) , the total output power at $i_h(x, y)$ is

$$P_1(U, V) = \int_{-\infty}^{\infty} \int_{-\infty}^{\infty} S_1(u, v) |H(u, v)|^2 dudv ,$$

or

$$P_1(U, V) = \int_{-\infty}^{\infty} \int_{-\infty}^{\infty} S_1(u, v) |G(u - U, v - V)|^2 dudv . \quad (7)$$

Equation (7) gives the total output power at $i_h(x, y)$ for a particular Gabor prefilter. It can be generalized, so that $P_1(u, v)$ can be calculated efficiently for all Gabor prefilter center frequencies (U, V) simultaneously. To see this, consider a window $w(x, y)$ as follows:

$$w(x, y) = g(x, y) * g(x, y) = \frac{1}{2\pi(\sqrt{2}\sigma_g)^2} e^{-\frac{(x^2+y^2)}{2(\sqrt{2}\sigma_g)^2}} , \quad (8)$$

where $g(x, y)$ is the Gaussian (1). Note that $w(x, y)$ is completely determined by parameter σ_g . From (1,3), the Fourier transform of $w(x, y)$ is:

$$\mathcal{F}\{g(x, y) * g(x, y)\} = [G(u, v)]^2 = e^{-4\pi^2\sigma_g^2(u^2+v^2)} ,$$

where $\mathcal{F}\{\}$ denotes the Fourier transform operator. We can now compute $P_1(u, v)$ for all frequencies (u, v) by taking the Fourier transform of the windowed autocorrelation $w(x, y)R_1(x, y)$

$$P_1(u, v) = \mathcal{F}\{w(x, y)R_1(x, y)\} = [G(u, v)]^2 * S_1(u, v) ,$$

or

$$P_1(u, v) = \int_{-\infty}^{\infty} \int_{-\infty}^{\infty} S_1(\alpha, \beta) |G(u - \alpha, v - \beta)|^2 d\alpha d\beta \quad (9)$$

where we use the fact that $[G(u, v)]^2 = |G(u, v)|^2$. From Parseval's theorem, $P_1(u, v)$ may be interpreted as the total output power of $i_h(x, y)$ for a Gabor prefilter with center frequency (u, v) and parameter σ_g . This can be easily seen by a comparison of (7) and (9). Relation (9) can be efficiently implemented in a discrete form using the FFT. The discrete form then gives $P_1(u, v)$ at a discrete set of center frequencies (u, v) and a particular σ_g .

When the foregoing analysis is applied to both textures, $t_1(x, y)$ and $t_2(x, y)$, it leads to the filter-design algorithm summarized below:

1. Estimate the autocorrelations, $R_1(x, y)$ and $R_2(x, y)$, of the two textures of interest using the given realizations of the textures, t_1 and t_2 .
2. Form the window function $w(x, y)$ in (8) for a given Gabor prefilter parameter σ_g .

3. Compute $P_1(u, v)$ and $P_2(u, v)$ for the two textures using a discrete FFT implementation of (9).
4. Choose the center frequency that maximizes the ratio of $P_1(u, v)$ to $P_2(u, v)$ as follows:

$$(U, V) = \arg \left\{ \max_{(u, v)} \left(\frac{P_1(u, v)}{P_2(u, v)} \right) \right\} \quad (10)$$

5. Repeat steps 2 through 4 for all σ_g under consideration.
6. Select the Gabor prefilter, specified by (U, V, σ_g) , that gives the best segmentation error performance, based on criteria discussed in Part 4.

The above algorithm gives a Gabor prefilter that emphasizes texture t_1 over t_2 in the output i_h ; i.e., the average energy in the filtered output is greater for t_1 than t_2 . The filter is optimal in the sense that it maximizes the expected ratio of average output energy for the two Gabor prefiltered textures. Similarly we could maximize the ratio $P_2(u, v)/P_1(u, v)$, resulting in a filter that emphasizes t_2 over t_1 . In practice, we chose the the filter associated with the larger of the two maximum power ratios $P_1(u, v)/P_2(u, v)$ or $P_2(u, v)/P_1(u, v)$.

The output power in (7) is equivalent to the second moment of the Gabor prefiltered output. Hence, (10) may also be interpreted in a statistical sense as maximizing the ratio of the second moments of the filtered textures. Dunn and Higgins have shown that $m(x, y)$ in (4) has a Rician pdf for many textures.^(5,7) The total output power, because of its statistical interpretation as the second moment, establishes bounds on the mean and variance of the Rician-distributed Gabor-prefilter output $m(x, y)$. Thus, a large power ratio should correspond to lower classification error, since this implies that the ratio of the average energy for the two filtered textures will be larger. Later, in the results of Part 5, a large power ratio is shown to correspond to a large contrast between the average intensities of the filtered textures. Using a Gabor prefilter with a large ratio of $P_1(u, v)/P_2(u, v)$ results in a filtered image where the region corresponding to texture t_1 is much brighter than the region corresponding to t_2 .

A significant benefit of the proposed filter-design algorithm is that it is far more efficient computationally than the previously proposed optimal approach.^(5,7) The computational complexity of new method is primarily driven by the computation of $P(u, v)$ in (9). First, $R(x, y)$ is computed as a size $2Nx2N$ acyclic autocorrelation using the operation $\mathcal{F}^{-1}\{|\mathcal{F}\{t_z\}|^2\}$ where t_z is the zero-padded version of the size NxN sample texture. Second, $P(u, v)$ is calculated as $\mathcal{F}\{w(x, y)R_1(x, y)\}$ using an NxN window for $w(x, y)$. These two steps are implemented as two $2Nx2N$ FFT's and one NxN FFT with a computational complexity of $O(9N^2 \log_2 N)$.

The most direct comparison in computational complexity is with the work of Dunn and Higgins, since this is the only other approach considering the design of a single filter to segment two textures.^(5,7) The computational complexity of the approach proposed by Dunn and Higgins is primarily driven by the need to perform ≈ 200 2-dimensional Gaussian-windowed FFT's (Fast Fourier Transforms) on each sample texture, i.e. t_1 and t_2 . This results in a computational complexity of $O(200N^2 \log_2 N)$ for size NxN sample texture images. Thus, the new method is approximately 22 times less complex than the method of Dunn and Higgins.

4. ESTIMATION OF FILTER OUTPUT STATISTICS

The previous section presented an efficient algorithm for designing the Gabor prefilter $h(x, y)$. This section discusses how to estimate the statistics of $m(x, y)$ and $m_p(x, y)$, so that a threshold on $m_p(x, y)$ can be set that minimizes the image-segmentation error. An algorithm is developed to estimate the pdf's of the Gabor-prefilter and Gaussian-postfilter outputs, $m(x, y)$ and $m_p(x, y)$. Once the output distributions for the two textures of interest are known, it is straightforward to calculate a threshold that minimizes image-segmentation error. Although the Gabor-prefilter and Gaussian-postfilter output statistics could be directly estimated from the filtered images, the new method presented below offers a new and efficient approach to the single-filter multi-texture and multi-filter multi-texture Gabor filter design problem. These issues are briefly discussed later, and some preliminary results using these new approaches have been recently presented!⁽²⁰⁾

We first discuss a signal model that provides a framework for estimating the pdf of the Gabor-prefilterer output $m(x, y)$ from the autocorrelation of a texture, or more precisely from an expression of the form (9). Dunn and Higgins have shown the prefilterer output to be characterized well by a Rician distribution.^(5, 7, 21) For simplicity, we retain the 1-dimensional notation of Dunn and Higgins, and represent the Gabor prefiltered output $i_h(x, y)$ as $i_h(x)$. Later we generalize the 1-dimensional results to the 2-dimensional case. A Gabor prefiltered texture with random perturbations is shown to be modeled by^(5, 7)

$$i_h(x) = [(A_0 \cos(\theta) + X(x)) + j(A_0 \sin(\theta) + Y(x))] e^{j2\pi(Ux)},$$

where A_0 is the magnitude of the sinusoidal component of the Gabor prefiltered image due to the unperturbed texture. $X(x)$ and $Y(x)$ are independent, zero-mean, Gaussian lowpass random processes due to the perturbations in the texture. Rearranging:

$$i_h(x) = A_0 e^{j2\pi Ux + \theta} + (X(x) + jY(x)) e^{j2\pi(Ux)}. \quad (11)$$

Hence, the Gabor prefiltered image is modeled as a complex exponential $s(x, y)$ due to the first term in (11), and bandpass noise $n(x, y)$ due to the second term. Extending this to two dimensions, the model for the Gabor prefiltered image becomes

$$i_h(x, y) \approx s(x, y) + n(x, y) = A e^{-j2\pi(Ux + Vy)} + n(x, y) \quad (12)$$

The phase term θ is not included in (12) since phase information is not used in the proposed methods, and the position of constituent textures in the input image is generally unknown.

The frequency domain representation of $i_h(x, y)$ consists of an impulse at the center frequency of the complex exponential plus bandlimited noise shaped by the Gabor prefilter $H(u, v)$. In (12) the Gabor prefilter $h(x, y)$ bandlimits the input $i(x, y)$ such that the prefiltered image $i_h(x, y)$ essentially consists of a small bandwidth around the center frequency (U, V) of the prefilter. In practice, the Gabor prefilter often focuses on a significant spectral peak of a texture. Thus, the output signal $i_h(x, y)$ in this small passband is modeled as a single dominant complex exponential plus complex bandpass noise. Strongly periodic components of a texture would tend to be represented by larger values of A .

Given the model (12), it is well known that $m(x, y)$, the magnitude of the complex signal $i_h(x, y)$, has a Rician distribution $p(m)$ when $n(x, y)$ is Gaussian bandlimited noise; i.e.,

$$p(m) = \frac{2m}{N} e^{-\left(\frac{m^2 + A^2}{N}\right)} I_0\left(\frac{2mA}{N}\right) \quad (13)$$

where $m \in m(x, y)$, A is the amplitude of the complex exponential, $I_0(\cdot)$ is the modified Bessel function of the first kind with zero order, and N is the total noise power.^(5, 7, 21) The distribution is completely determined by the values of A and N .

When $A \ll N$ (or $A \approx 0$), $p(m)$ approaches a Rayleigh distribution.⁽²¹⁾ Hence, the Rician model in (13) accommodates situations in which the output statistics follow a Rayleigh distribution. In the Rayleigh case, the power spectrum of $i_h(x, y)$ is dispersed across the passband almost uniformly and does not have a concentration (or peak) at any particular frequency within the passband. As it turns out, our results indicate that the filter design algorithm tends to favor selecting $h(x, y)$ such that the filtered version of t_1 in $m(x, y)$ will be Rician with $A \not\approx 0$, while the corresponding filtered version of t_2 in $m(x, y)$ will be approximately Rayleigh with $A \approx 0$. This effect is a consequence of the maximum ratio in (10). The ratio is commonly maximized at the frequency of a dominant sinusoidal component in one of the two textures. Since it is unlikely that both textures will have a dominant sinusoid at the same frequency, the other prefiltered texture tends to be Rayleigh distributed.

Equation (12) is used to estimate the output statistics of $m(x, y)$ from $P_1(u, v)$. To do this, we first observe that the Gabor prefiltered image $i_h(x, y)$ in (12) is the result of the bandpass filtering operation.

Since the Gabor prefilter $h(x, y)$, which is determined by (U, V, σ_g) , passes spatial frequencies localized around the center frequency (U, V) and rejects energy at other frequencies, a *locally* equivalent model (in the spatial-frequency plane) at the *input* of the Gabor prefilter is a complex exponential plus white noise, with power spectral density $S_1(u, v)$:

$$\begin{aligned} S_1(u, v) &\approx \mathcal{F}\{R_1(x, y)\} \\ &\approx A^2\delta(u - U, v - V) + \frac{\eta}{4} \end{aligned} \quad (14)$$

where the uniform power density η is used to model the spectral components at the Gabor prefilter input which contribute to $n(x, y)$ in (12). We emphasize that this model of the power spectrum of $i(x, y)$ is only valid within the approximate passband of the prefilter. When the input model (14) is applied to (9) of the filter design algorithm, we get

$$P_1(u, v) \approx A^2 e^{-4\pi^2\sigma_g^2[(u-U)^2+(v-V)^2]} + \frac{\eta}{16\pi\sigma_g^2}. \quad (15)$$

In (15) the first term arises from the dominant sinusoid in $i(x, y)$ that lies within the Gabor prefilter passband; i.e., the $\delta(u - U, v - V)$ term in (14). The second term arises from the remaining power in $i(x, y)$ that lies within the Gabor prefilter passband; i.e., the $\delta(u - U, v - V)$ term in (14). This second term gives the parameter N in (13):

$$N = \eta/(16\pi\sigma_g^2). \quad (16)$$

The Rician parameters A and N may be estimated from (15). Denote the power for texture t_1 at Gabor prefilter center frequency (U, V) as P_0 . The half power point of $P_1(u, v)$ in the absence of noise occurs at a frequency offset of $\nu = \sqrt{\ln(2)}/(2\pi\sigma_g)$. Then,

$$\begin{aligned} P_0 &\approx P_1(U, V) = A^2 + N, \\ P_\nu &\approx P_1(U \pm \nu, V) = A^2 e^{-4\pi^2\sigma_g^2[(\sqrt{\ln(2)}/(2\pi\sigma_g))^2]} + \frac{\eta}{16\pi\sigma_g^2} = \frac{A^2}{2} + N \end{aligned} \quad (17)$$

which gives relations for the Rician parameters:

$$A^2 \approx 2(P_0 - P_\nu), \quad N \approx 2P_\nu - P_0 \quad (18)$$

A frequency offset of $\nu = \sqrt{\ln(2)}/(2\pi\sigma_g)$ is used for illustration, other frequency offsets can be used in (17) with slight modifications in (18). Good results have been obtained with frequency offsets in the range of $.094/\sigma_g < \nu < .133/\sigma_g$.

Given A and N , the mean μ_g and variance s_g^2 of the prefilter output $m(x, y)$ can be calculated from the Rician pdf $p(m)$ in (13).

Finally, we can estimate the output statistics of $m_p(x, y)$ under varying degrees of Gaussian postfiltering. From (5) and (6), the Gaussian postfiltering process can be considered as a spatial averaging of independent samples of $m(x, y)$. The mean μ_p and variance s_p^2 of the Gaussian postfiltered output can then be approximated as

$$\mu_p = \mu_g, \quad s_p^2 = \frac{s_g^2 \sigma_g^2}{\sigma_p^2}. \quad (19)$$

For small ratios of σ_g^2/σ_p^2 , the Gaussian postfiltered output pdf will become approximately Gaussian, due to the central limit theorem. Therefore, for texture t_i , the pdf $p_i(m_p)$ of the Gaussian-postfilter output $m_p(x, y)$ is approximated as

$$p_i(m_p) = \frac{1}{\sqrt{2\pi s_{pi}^2}} e^{-\frac{(m_p - \mu_{pi})^2}{2s_{pi}^2}}$$

where μ_{pi} and s_{pi}^2 are the mean and variance of the Gaussian-postfilter output for texture t_i . The optimal image-segmentation threshold τ is then selected by modeling the output density of $i_s(x, y)$ as a bimodal Gaussian distribution having equal *a priori* probabilities for the two textures; τ is selected such that

$$p_1(\tau) = p_2(\tau). \quad (20)$$

Equation (20) is well known to be reducible to a quadratic in τ having a closed form solution.⁽²²⁾ In the event of two distinct solutions, the solution between μ_1 and μ_2 is chosen.

The foregoing arguments provide new insight into the need for postfiltering. The effect of Gaussian postfiltering is particularly pronounced as the ratio A/N becomes small. The Rician pdf approaches a Rayleigh pdf with small ratios of A/N , and the Rayleigh pdf exhibits longer tails. The long tails on the Rayleigh distribution lead to large image-segmentation errors when postfiltering is not employed. Hence, postfiltering is particularly important for segmenting textures having no dominant sinusoid within the passband of the Gabor prefilter. Furthermore, it is unlikely that a Gabor prefilter will pass dominant sinusoids for *both* textures t_1 and t_2 , and so *at least one of the prefiltered textures is likely to have a Rayleigh distribution*. The inclusion of Gaussian postfiltering in the proposed methods enables a balanced treatment of Rician and Rayleigh distributed outputs.

The method also provides insight to the tradeoffs of Gabor prefiltering, Gaussian postfiltering, and spatial resolution. A given spatial resolution can be achieved by various combinations of Gabor prefilter bandwidth and Gaussian postfilter bandwidth. For noise-like textures ($A \approx 0$) with relatively flat power spectral densities, the Gabor prefilter output statistics will have approximately Rayleigh statistics regardless of the prefilter bandwidth set by σ_g . Also, the second moment (or power) of the output will be inversely proportional to σ_g^2 as shown in (16). For small ratios of σ_g/σ_p , the spatial localization is approximately set by the Gaussian postfilter. Using (16) and $A = 0$, the mean and standard deviation for a Rayleigh distributed output is⁽²¹⁾

$$\mu_g = \frac{\sqrt{\eta}}{8\sigma_g}, \quad s_g = \sqrt{1 - \frac{\pi}{4}} \left(\frac{\sqrt{\eta}}{4\sqrt{\pi}\sigma_g} \right).$$

where μ_g denotes the mean value of $m(x, y)$ and s_g denotes the standard deviation of $m(x, y)$. Then, using (19), the Gaussian-postfilter output's mean μ_p and standard deviation s_p are

$$\mu_p \approx \frac{\sqrt{\eta}}{8\sigma_g}, \quad s_p \approx \sqrt{1 - \frac{\pi}{4}} \left(\frac{\sqrt{\eta}}{4\sqrt{\pi}\sigma_p} \right)$$

and

$$\frac{s_p}{\mu_p} \approx \frac{2\sigma_g}{\sigma_p} \sqrt{\frac{4 - \pi}{\pi}}.$$

Hence, for a fixed spatial resolution set by σ_p , it is advantageous to use a small value of σ_g (large Gabor prefilter bandwidth) to reduce the ratio of the standard deviation to the mean of the Gaussian postfiltered output. This effectively results in increasingly narrow pdf's for the Gaussian postfiltered output with decreasing ratios of σ_g/σ_p for the case of noise-like textures with relatively flat local power spectral densities.

The following is a summary of the algorithm for estimating the output distributions for $m(x, y)$ and $m_p(x, y)$ and selecting a segmentation threshold:

1. Obtain P_0 and P_ν from $P_1(u, v)$ and $P_2(u, v)$, using (17) with (U, V) from (10).
2. Calculate A and N for both textures, using (18).
3. For each texture, estimate the pdf of $m(x, y)$ by substituting the estimates of A and N into (13). Calculate the means and variances of $m(x, y)$ for both textures from their pdf's.
4. Pick σ_p and calculate Gaussian-postfilter output statistics using σ_g^2/σ_p^2 in (19), with the Gabor-prefilter output means and variances from step 3.
5. Set the image-segmentation threshold τ , using (20).
6. Repeat steps 4 and 5 for each σ_p^2 of interest.
7. Choose the best compromise between the image resolution (determined by σ_p) and image-segmentation error (determined by σ_g^2/σ_p^2).

Note that the foregoing algorithm is not necessarily limited to the center-frequency (U, V) chosen by the frequency-selection algorithm. This observation that the statistics can be estimated at any frequency leads to alternative Gabor filter design approaches that are the subject of ongoing research.^(17,18) Thus, even though it is apparent that the empirical distributions of the filtered textures could be used to directly establish the segmentation threshold, we chose to employ the foregoing method to estimate output statistics since it leads to useful approaches to the more difficult multi-filter multi-texture design problem. However, by choosing a peak power point from (10), the frequency-selection algorithm tends to choose a center frequency that should be well represented by the presumed model (14).

5. RESULTS

The new algorithms were tested on a range of Brodatz⁽²³⁾ and synthetic texture images. All images used were 256x256 pixel 8-bit gray-scale images. The mean values of all textures were equalized so that segmentation based on average gray scale was not possible. In each example a single value of σ_g and σ_p are used to illustrate the effectiveness of the selected Gabor prefilter center-frequency and the output statistical estimates. For guidelines on selecting values for σ_g , see Dunn *et al.*⁽⁶⁾ In the following examples, σ_p was chosen to be twice as large as σ_g so that the effect of Gaussian postfiltering was clearly visible.

Figure 2 presents results for a pair of Brodatz textures using the Gabor prefilter designed with the new algorithm. The 256x256 input image $i(x, y)$ in Fig. 2(a) consists of a central d77 "cotton canvas" texture region superimposed on a background of the d16 "herringbone weave" texture. The prefilter output $m(x, y)$ is shown in Fig. 2(b). The measured histograms of $m(x, y)$ are shown in Fig. 2(c) as solid lines, and the predicted Rician pdf's using (13) are shown as dashed lines. The curves that peak at lower output amplitude correspond to the dark outer border (prefiltered d16) of Fig. 2(b), and the curves which peak at the larger amplitude correspond to the bright central region (prefiltered d77) of Fig. 2(b). The measured output statistics are seen to correspond well with the predicted Rician statistics.

The Gaussian-postfilter output m_p , where $\sigma_g/\sigma_p = 0.5$, is shown in Fig. 2(d). The predicted Gaussian pdf (dashed lines) and measured output histograms (solid lines) are presented in Fig. 2(e) for the Gaussian postfiltered image. The segmented image $i_s(x, y)$ is shown in Fig. 2(f) for the postfiltered output using the optimal threshold. The Gaussian postfiltering reduces the tails of the measured histograms, as is evident from comparing Fig. 2(c) and 2(e). A large amount of overlap is seen in the Gabor prefilter histograms of Fig. 2(c). It is apparent that a segmentation without postfiltering will result in a large segmentation error, and this is confirmed in Fig. 2(g). The histogram overlap is virtually eliminated by Gaussian postfiltering. This results in low error for the segmented image of Fig. 2(f). Finally, the results of a segmentation using the method of Dunn and Higgins are shown in Fig. 2(h) for comparison.^(5,7) The same σ_p and σ_g were used, but a different center-frequency $(U, V) = (0, .195)$ was selected. Although the filter center-frequencies differ,

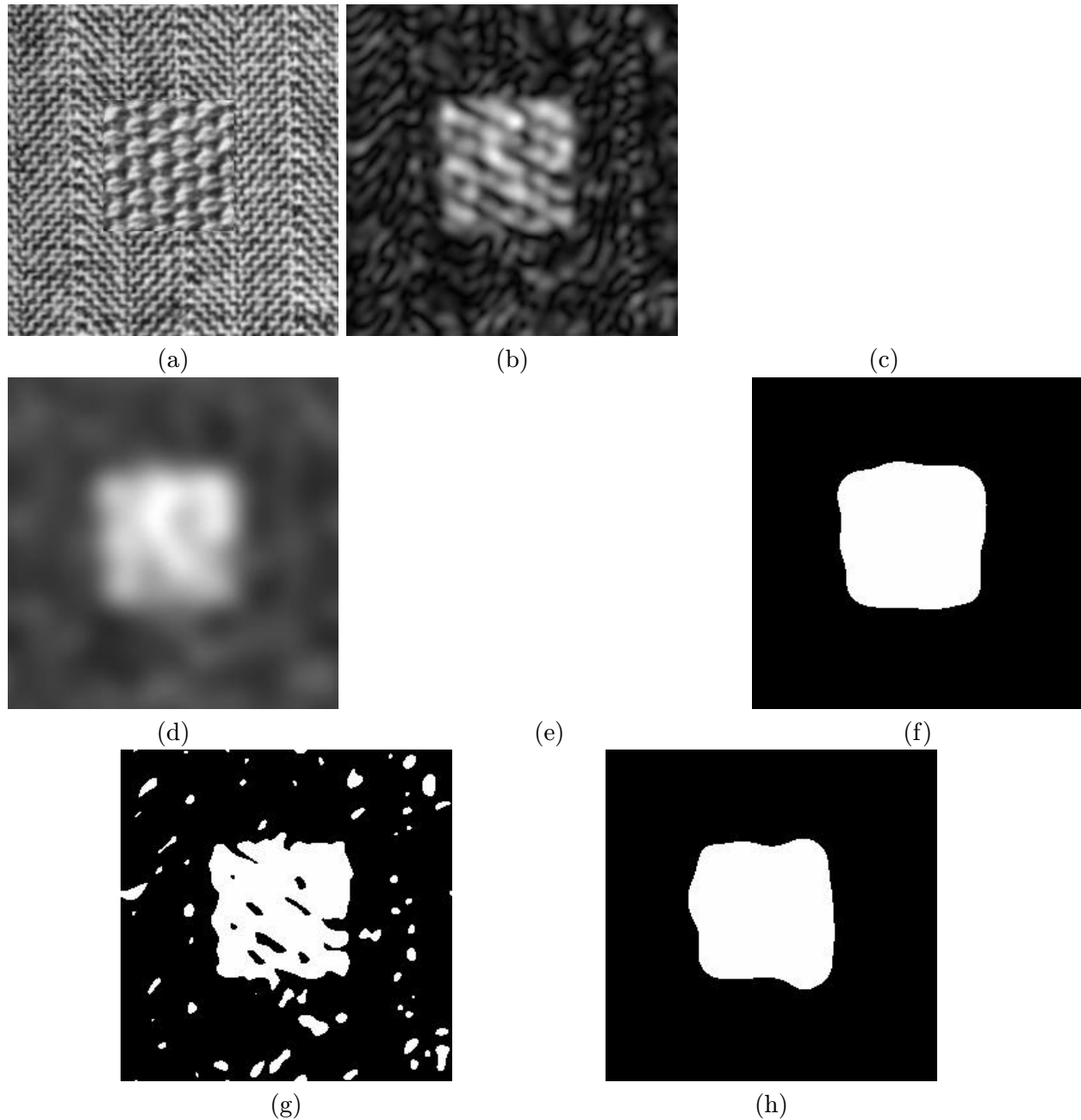


Figure 2: Results for optimal filter: (a) Input composite image: d16 “herringbone weave” (border) d77 “cotton canvas” (center). (b) Prefilter magnitude $m(x, y)$, $(U, V) = (-.035, -.047)$ cycles/pixel, $\sigma_g = 5$. (c) Histogram of predicted (dashed) and actual (solid) $m(x, y)$. (d) Postfiltered output $m_p(x, y)$, $\sigma_p = 10$. (e) Histogram of predicted (dashed) and actual (solid) $m_p(x, y)$. (f) Segmentation of postfiltered output, threshold = 10. (g) Segmentation of prefiltered output, threshold = 11. (h) Segmentation of postfiltered output using previous algorithm,^(5,7) $\sigma_g = 5$, $\sigma_p = 10$, $(U, V) = (0, .195)$.

both methods are seen to generate effective filters for segmentation.

Fig. 3 presents results for a pair of noise-like textures. The two textures are comprised of essentially

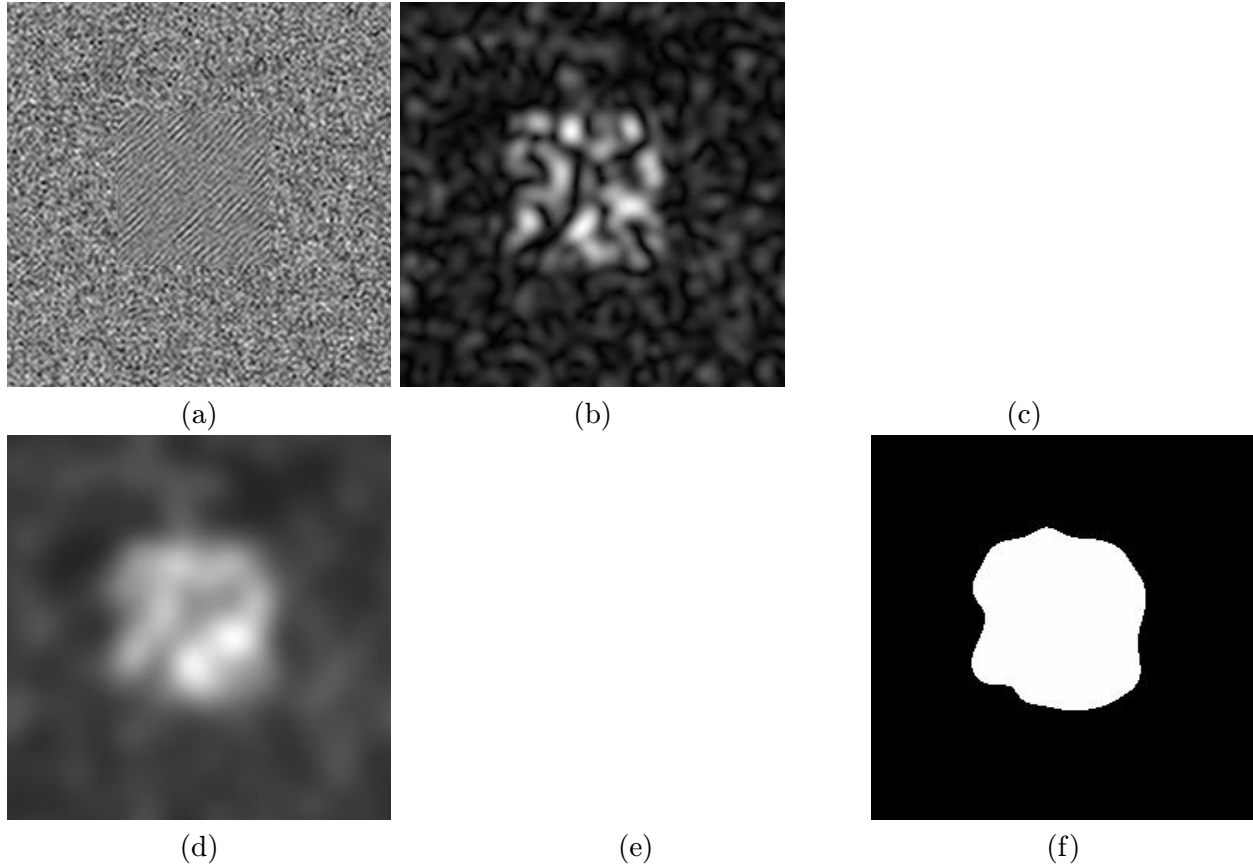


Figure 3: Results for optimal filter: (a) Input composite image: uniform noise (border) and uniform noise with enhanced diagonal energy (center). (b) Prefilter magnitude $m(x, y)$, $(U, V) = (-.16, -.16)$ cycles/pixel, $\sigma_g = 5$. (c) Histogram of predicted (dashed) and actual (solid) $m(x, y)$. (d) Postfiltered output, $\sigma_p = 10$. (e) Histogram of predicted (dashed) and actual (solid) $m_p(x, y)$. (f) Segmentation of postfiltered output, threshold = 5.3.

flat power spectral densities, except that the central texture of Fig. 3(a) has increased power density along the diagonal direction. The power density is increased at a frequencies of $(-.16, -.16)$ and $(+.16, +.16)$ cycles/pixel over a passband of .08 cycles per pixel. The histograms of Fig. 3(c) have a Rayleigh appearance, as expected for the envelope of bandpass noise. By construction, these two synthetic textures have no dominant spatial-frequency components. Comparison of the histogram overlaps in Fig. 3(c) and 3(e) reveals the importance of Gaussian postfiltering. The long tails of the Rayleigh pdf associated with noise-like textures, as Fig. 3(c) demonstrates, leads to a large segmentation error in the absence of postfiltering. Although the histograms of the Gaussian postfiltered output show great improvement over the Gabor-prefilter output histograms, the borders of the segmentation in Fig. 3(f) appear worse than the results of Fig. 2. This error is a consequence of the low ratio of average powers, per (10), combined with the Rayleigh prefilter output pdf's. Comparing Figs. 2(c) and 3(c), we can make two observations. First, the means for Fig. 2 are 5.6 and 20.4 with a ratio of 3.7, while the means for Fig. 3 are 3.2 and 9.9 with a ratio of 3.1. Second, the lower and upper distributions in Fig. 2(c) have $A/N = 0$ and $A/N = .12$, respectively, while in Fig. 3(c) $A/N = 0$ for both the lower and upper distributions. Thus, the segmentation in Fig. 2 is expected to be better than Fig. 3, because the constituent textures have a larger ratio of output means and a larger ratio of A/N in the upper pdf.

Figure 4 presents results for another Brodatz texture pair. The input image in Fig. 4(a) consists of texture d77 “cotton canvas” imposed on a background of d9 “grass.” The Gabor-prefilter output in Fig. 4(b)

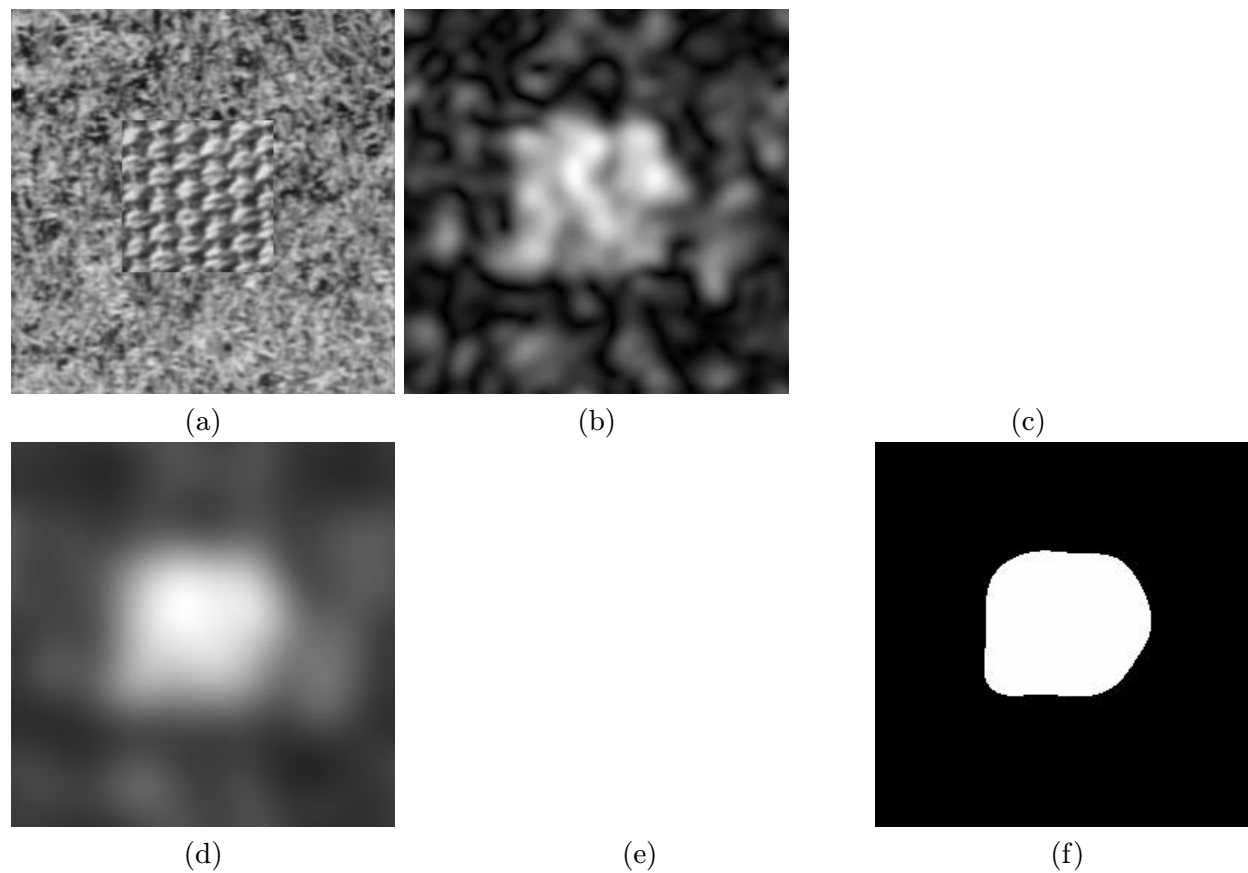


Figure 4: Results for optimal filter: (a) Input composite image: d9 “grass” (border) and d77 “cotton canvas” (center). (b) Prefilter magnitude $m(x, y)$, $(U, V) = (-.035, -.055)$ cycles/pixel, $\sigma_g = 8$. (c) Histogram of predicted (dashed) and actual (solid) $m(x, y)$. (d) Postfiltered output, $\sigma_p = 16$. (e) Histogram of predicted (dashed) and actual (solid) $m_p(x, y)$. (f) Segmentation of postfiltered output, threshold =9.9.

is seen to emphasize the central texture while suppressing the outer texture (darker response). The mottled appearance of the response to the grass texture is characteristic of a Rayleigh distribution, and is also evidenced in the apparent Rayleigh shape of the corresponding histogram (mean ≈ 5) in Fig. 4(c). Rician distributions approach a Gaussian distribution for $A \gg N$, and the histogram of the cotton canvas appears more Gaussian than Rayleigh. In Fig. 4(c) $A/N = .38$ for the upper pdf and $A/N = .02$ for the lower pdf. The Gaussian postfiltered image and associated histograms are in Figs. 4(d) and 4(e). Again, the postfiltering is seen to greatly reduce the tails of the histograms. The segmented image in Fig. 4(f) is generated from the Gaussian postfiltered image in Fig. 4(d) using the threshold calculated in (20) from the predicted statistics. Note that σ_g and σ_p are larger in this example than for Figs. 2 and 3, resulting in increased spatial smoothing and increased frequency selectivity at the expense of reduced spatial localization.

Section 3 pointed out that the filter-design algorithm is much more efficient than the previously proposed method.^(5,7) It is important, however, to determine how the filters designed by the two methods compare. Figure 5 gives such a comparison.

$P_1(u, v)/P_2(u, v)$ is shown in Fig. 5 for the “d16-d77” example of Fig. 2. The intensity in Fig. 5 is logarithmically proportional to $P_1(u, v)/P_2(u, v)$ with $(u, v) = (0, 0)$ at the center and the positive u and v axes labeled. The black box surrounds the point at which $P_1(u, v)/P_2(u, v)$ is maximum, and the white box surrounds the minimum. Black “pluses” are the most highly rated frequencies selected by the previous method.^(5,7) Although the selected frequencies in this example are not identical, the tendency of both

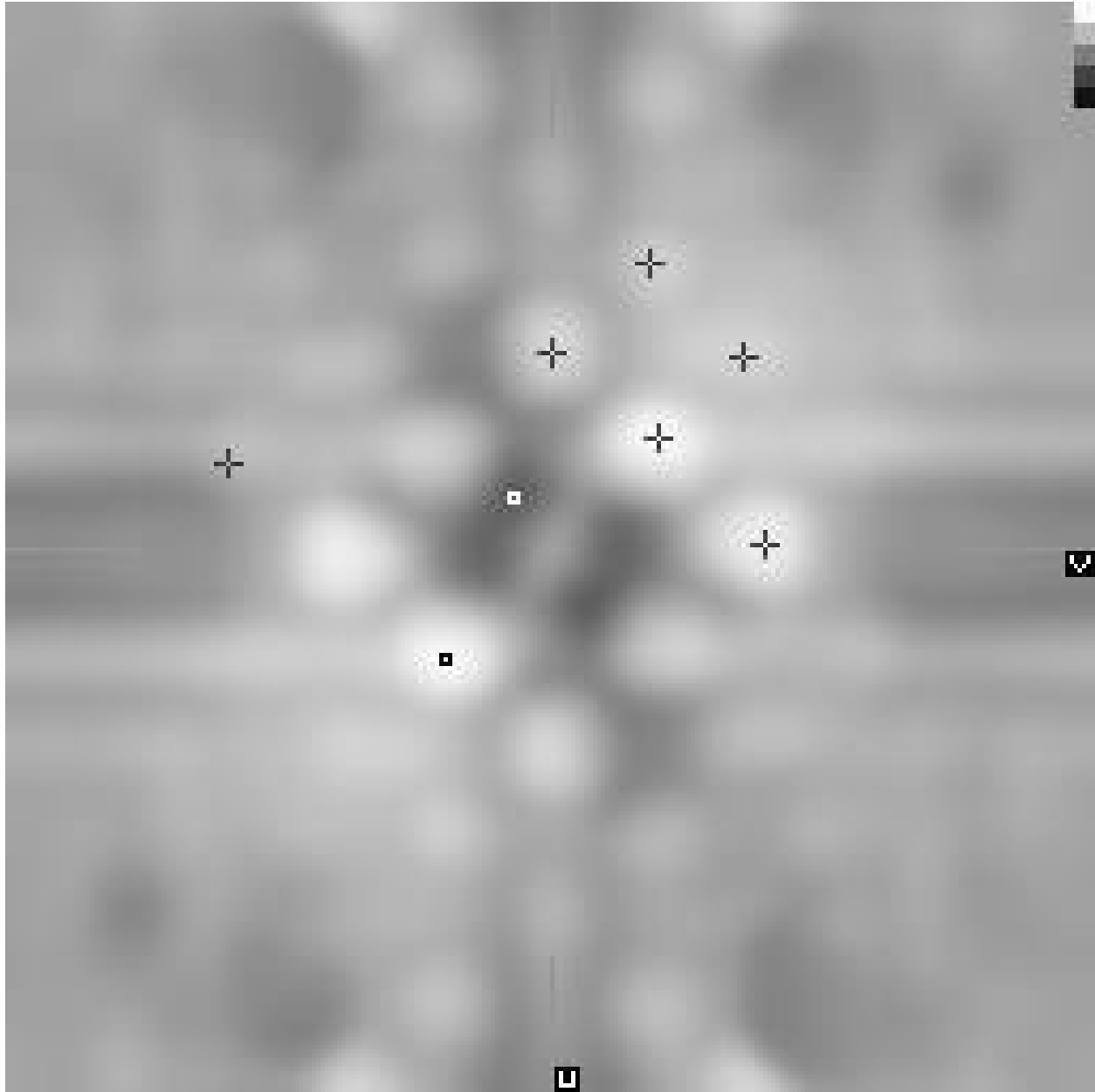


Figure 5: $P_1(u, v)/P_2(u, v)$ for the example of Fig. 2, d16 “herringbone weave” (border) d77 “cotton canvas” (center). The intensity is logarithmically proportional to $P_1(u, v)/P_2(u, v)$, the center corresponds to $(u, v) = (0, 0)$, and the lower right corner corresponds to positive u and v . The black and white boxes surround the maximum and minimum $P_1(u, v)/P_2(u, v)$ respectively, which correspond to the center frequencies selected by the proposed filter-design algorithm. The +’s correspond to frequencies selected by the previous algorithm.^(5,7)

methods to select peaks in $P_1(u, v)/P_2(u, v)$ is readily apparent. In other cases, the method of Dunn and Higgins is seen to select minima in $P_1(u, v)/P_2(u, v)$ (equivalent to maxima in $P_2(u, v)/P_1(u, v)$) such as that indicated by the white box.

The proposed method’s improvement in computational complexity is obtained at the cost of some loss in the information used to set the filter center frequency. The proposed method selects the Gabor prefilter center

frequency based on a measure of total power (knowledge of the second moment of the output distribution), whereas the previous method^(5,7) completely characterizes the distribution with estimates of A and N (which determine the pdf). Thus, the two algorithms do not necessarily select the same center frequencies because differences in $P_1(u, v)/P_2(u, v)$ can be offset by differences in A^2/N . However, both algorithms are seen to generate effective filters.

In the previous examples, the Gabor-prefilter output was represented well by the Rician pdf, and the Gaussian-postfilter output was represented well by the Gaussian pdf. These results are, however, dependent on the choice of σ_g and σ_p . At one extreme, with large σ_g , the prefilter output consists of a single spectral component from the FFT of each input texture. This single sinusoid with its constant envelope results in a zero-variance output pdf, regardless of σ_p . At the other extreme, with small σ_g , the Gabor-prefilter output approaches the original input texture. As the prefilter output statistics approach the statistics of the input image, they are not likely to be well modeled as a Rician pdf. In this latter extreme, however, a Gaussian postfilter may provide sufficient smoothing such that the postfilter output approaches a Gaussian distribution.

The input textures also affect the overall segmentation performance. The previous examples include a variety of natural and noise-like textures which have some degree of randomness. Uniform textures, on the other hand, do not have this random component, and can be represented as a Fourier series expansion.⁽⁶⁾ Prefiltered uniform textures often exhibit low variances and large ratios of $P_1(u, v)/P_2(u, v)$. In such situations, the ratio of the mean Gabor-prefilter output to the segmentation threshold can become large (≈ 10). This leads to segmentation error at texture boundaries when the filtered image makes the transition from the region with the large mean value to the region with the smaller mean value. Even so, the proposed method produces effective filter designs for uniform textures in most situations.

6. CONCLUSION

The new Gabor prefilter design method is optimal in the sense that the resulting prefilter maximizes the ratio of expected average output energy for the two textures. This results in large differences in the “brightness” of regions composed of different textures in the Gabor prefiltered image. Furthermore, the Gabor prefilter design method has significant computational advantages over previous approaches. We also described an algorithm for estimating output statistics and for setting segmentation thresholds. The estimation of Gabor prefilter and Gaussian-postfilter output statistics is demonstrated in several examples for natural and synthetic textures. Effective segmentation thresholds and image segmentations are generated using the Gaussian statistical model for Gaussian postfiltered outputs. In addition, the algorithms provide new insight into the need for postfiltering and the treatment of noise-like textures.

Remaining issues in the design of Gabor filters for texture segmentation include the design of a single filter to segment multiple (> 2) textures and the design of multiple filters to segment multiple textures. The present work provides several steps toward these two objectives. First, the method of estimating output statistics from the windowed autocorrelation (or power spectrum) of the sample textures is computationally efficient. This computational efficiency becomes increasingly important as the size of images, number of Gabor prefilters, number of Gaussian postfilters, and number of textures increases. Second, the method provides insight into the tradeoffs of Gabor prefiltering, Gaussian postfiltering, and spatial resolution. Finally, new work is being done on a hybrid method that combines the method for prefilter center-frequency selection with the method for output pdf estimation. Preliminary results on this hybrid method for the single-filter multi-texture design problem confirm the utility of the foregoing methods in developing new approaches to the single-filter multi-texture and multi-filter multi-texture Gabor filter design problem.⁽²⁰⁾

The previous discussion has focused on the design of Gabor filters. The methods, however, should be applicable to other types of filters. This may be accomplished by replacing the kernel $G(u, v)$ in (9) by a different kernel $K(u, v)$. The only caveat is that necessary properties of $G(u, v)$ used in the foregoing derivations set restrictions on $K(u, v)$. In particular, $K(u, v)$ should satisfy $[K(u, v)]^2 = |K(u, v)|^2$ as used in (9), and $K(u, v)$ should be non-negative to assure that the spectral estimate given by (9) is non-negative.

Acknowledgements — This work was partially supported by NIH FIRST award #CA53607 from the National Cancer Institute of the National Institutes of Health. Portions of this manuscript were presented at the conference.⁽²⁴⁾

References

1. A. C. Bovik, M. Clark, and W. S. Geisler, Multichannel texture analysis using localized spatial filters, *IEEE Trans. Pattern Anal. Machine Intell.*, **12**, 55–73, (1990).
2. A. C. Bovik, Analysis of multichannel narrow-band filters for image texture segmentation, *IEEE Trans. Signal Processing*, **39**, 2025–2043, (1991).
3. A. K. Jain and F. Farrokhnia, Unsupervised texture segmentation using Gabor filters, *Pattern Recognition*, **23**, 1167–1186, (1991).
4. A. C. Bovik, N. Gopal, T. Emmoth, and A. Restrepo, Localized measurements of emergent image frequencies by Gabor wavelets, *IEEE Trans. Inform. Theory*, **38**, 691–711, (1992).
5. D. F. Dunn and W. E. Higgins, Optimal Gabor-filter design for texture segmentation, *Proc. IEEE Int. Conf. Acoust., Speech, Signal Processing*, vol. V, V37–V40, (1993).
6. D. Dunn, W. Higgins, and J. Wakeley, Texture segmentation using 2-D Gabor elementary functions, *IEEE Trans. Pattern Anal. Machine Intell.*, **16**, 130–149, (1994).
7. D. F. Dunn and W. E. Higgins, Optimal Gabor filters for texture segmentation, *IEEE Trans. Image Proc.*, **4**, 947–964, (1995).
8. J. Bigun and J. M. H. du Buf, N-folded symmetries by complex moments in Gabor space and their application to unsupervised texture segmentation, *IEEE Trans. Pattern Anal. Machine Intell.*, **16**, 80–87, (1994).
9. A. K. Jain and S. Bhattacharjee, Text segmentation using Gabor filters for automatic document processing, *Machine Vision and Applications*, **5**, 169–184, (1992).
10. R. Mehrotra, K. R. Namuduri, and N. Ranganathan, Gabor filter-based edge detection, *Pattern Recognition*, **25**, 1479–1493, (1992).
11. J. G. Daugman, High confidence visual recognition of persons by a test of statistical independence, *IEEE Trans. Pattern Anal. Machine Intell.*, **15**, 1148–1160, (1993).
12. M.-T. Leung, W. E. Engler, and P. Frank, Fingerprint image processing using neural network, *IEEE Reg 10 Conf. on Computer and Comm. Systems*, Hong Kong, 582–586, (1990).
13. J. G. Daugman, Complete discrete 2-D Gabor transforms by neural networks for image analysis and compression, *IEEE Trans. Acoust., Speech, Signal Processing*, **36**, 1169–1179, (1988).
14. T. Ebrahimi and M. Kunt, Image compression by Gabor expansion, *Optical Eng.*, **30**, 873–880, (1991).
15. M. Porat and Y. Zeevi, The generalized Gabor scheme of image representation in biological and machine vision, *IEEE Trans. Pattern Anal. Machine Intell.*, **10**, 452–468, (1988).
16. J. G. Daugman, Uncertainty relation for resolution in space, spatial frequency, and orientation optimized by two-dimensional visual cortical filters, *J. Opt. Soc. Amer. A*, **2**, 1160–1169, (1985).
17. T. P. Weldon, *Multiresolution Design of Multiple Gabor Filters for Texture Segmentation*. PhD thesis, The Pennsylvania State University, (1995).
18. T. Weldon and W. Higgins, Design of multiple Gabor filters for texture segmentation, to appear in *IEEE Int. Conf. Acous., Speech, Sig. Proc.*, Atlanta, GA, May 7-10, (1996).
19. D. F. Dunn, T. P. Weldon, and W. E. Higgins, Extracting halftones from printed documents using texture analysis, *Proc. IEEE Int. Conf. on Image Processing*, vol. II, (Lausanne, Switzerland), 225–228, (1996).
20. T. P. Weldon and W. E. Higgins, Multiscale Rician approach to Gabor filter design for texture segmentation, *IEEE Int. Conf. on Image Processing*, vol. II, (Austin, TX), 620–624, (13-16 Nov. 1994).

21. M. Schwartz, *Information Transmission, Modulation, and Noise*, third ed., McGraw-Hill, New York, NY, (1980).
22. R. C. Gonzalez and R. E. Woods, *Digital Image Processing*, Addison-Wesley, New York, NY, (1992).
23. P. Brodatz, *Textures: A Photographic Album for Artists and Designers*, Dover, New York, NY, (1966).
24. T. P. Weldon, W. E. Higgins, and D. F. Dunn, Efficient Gabor filter design using Rician output statistics, *IEEE Int. Symp. Circuits, Systems*, vol. 3, (London, England), 25–28, (30 May - 2 June 1994).

Biographical Sketches

Thomas Weldon received the B.S., M.Eng., and Ph.D. in electrical engineering from the Penn State in 1979, 1989, and 1995. From 1979 to 1982 he worked as a development engineer at Motorola in Plantation, Florida, where he designed portable communications equipment. From 1982 to 1984 he was a project engineer at Alpha Industries in Lansdale, Pennsylvania, where he designed high-frequency analog and digital microelectronic circuits. From 1984 to 1990 he was a senior engineer at American Electronic Laboratories in Lansdale, Pennsylvania, where he conducted research on advanced signal processing techniques and microwave communication systems. From 1990 to 1995 he was engaged in signal-processing and image-processing research at Penn State while completing his Ph.D. He is presently an assistant professor in the department of electrical engineering at the University of North Carolina at Charlotte, NC. His current research interests are image processing, signal processing, medical imaging, biotelemetry, cellular radio, and communication systems. He is a member of the Pattern Recognition Society, IEEE, and SPIE.

William E. Higgins obtained the B.S. degree in electrical engineering (1979) at the Massachusetts Institute of Technology and the M.S. (1981) and Ph.D. (1984) degrees in electrical engineering at the University of Illinois, Urbana. Previously, he worked as a principal research scientist at the Honeywell Systems and Research Center (1984-1987), Minneapolis, MN, working in the field of automatic target-recognition systems. He later was a senior research fellow in the Biodynamics Research Unit of the Mayo Clinic (1987-1989), Rochester, MN, working in the areas of multidimensional image analysis and visualization. Since 1989, he has been at the Pennsylvania State University, University Park, PA, where he is currently an associate professor in the departments of electrical engineering, computer science and engineering, and bioengineering. His research interests are in image processing, computer vision, scientific visualization, and medical image analysis. He is a member of the Pattern Recognition Society, IEEE, ACM, Sigma Xi, Tau Beta Pi, Eta Kappa Nu, and the SPIE.

Dennis Dunn received the B.S. degree in chemical engineering from Case Western Reserve University in 1969, the M.Eng. degree in engineering science from The Pennsylvania State University in 1981, and the Ph.D. degree in computer science from the Pennsylvania State University in 1992. He is presently an Assistant Professor with the Computer Science and Engineering Department, The Pennsylvania State University. His main research interests are computer vision, image processing, texture analysis, interpreting cursive text, and human-vision modeling.